European Journal of Immunology

Immunity to infection

Basic

Research Article

Dual role of monocyte-derived dendritic cells in *Trypanosoma cruzi* infection

Carolina V. Poncini[1,2] *and Stella M. González-Cappa*[1,2]

[1] Instituto de Investigaciones en Microbiología y Parasitología Médicas (IMPaM), Consejo Nacional de Investigaciones Científicas y Técnicas (CONICET)-Universidad de Buenos Aires, Argentina

[2] Departamento de Microbiología, Facultad de Medicina, Universidad de Buenos Aires, CABA, Argentina

Pathogens can cause inflammation when inoculated into the skin. The vector-transmitted protozoan parasite *Trypanosoma cruzi* induces poor cellular-infiltration and disseminates, causing high mortality in the experimental model. Here, we characterized the inflammatory foci at the parasite inoculation site and secondary lymphoid organs using a murine model. While no macrophages and few neutrophils and monocytes (Mo) were recruited into the skin, *T. cruzi* infection elicited the mobilization of Ly6C$^+$ Mo to draining lymph nodes and spleen. Over time, this population became enriched in CD11b$^+$Ly6C$^+$CD11c$^+$MHCII$^+$CD86$^+$ cells resembling inflammatory dendritic cells (DCs). Adoptive transfer of Ly6C$^+$ Mo purified from the bone marrow of *CD11c-GFP* transgenic mice confirmed the monocytic origin of Ly6C$^+$ DCs found in the spleen of infected animals. Isolated Mo-derived cells not only produced TNF-α and nitric oxide, but also IL-10 and displayed a poor capacity to induce lymphoproliferation. Ablation of Mo-derived cells by 5-fluorouracil confirmed their dual role during infection, limiting the parasite load by inducible nitric oxide synthase-related mechanisms and negatively affecting the development of anti-parasite T-cell response. This study demonstrated that consistent with their antagonistic properties, these cells not only control the parasite spreading but also its persistence in the host.

Keywords: Dendritic cells · Intradermal infection · Myeloid cells · Monocyte-derived cells · *Trypanosoma cruzi*

Additional supporting information may be found in the online version of this article at the publisher's web-site

Introduction

Trypanosoma cruzi is an intracellular protozoan parasite that affects millions of people in Latin America. During the last decade, it has been increasingly detected in North America and many European countries. Symptoms are variable, and Chagas disease occurs in one third of the infected patients. Experimental infection in mouse can be lethal. Nevertheless, a common feature in human and mouse infection is the anti-parasite response delayed in time [1].

In the host, *T. cruzi* trypomastigotes (Tp) invade nucleated cells. Macrophages (MC) are permissive to *T. cruzi* and are considered one of the first targets for parasite multiplication [2, 3]. However, the events occurring immediately after

Correspondence: Dr. Carolina V. Poncini
e-mail: cvponcini@gmail.com

T. cruzi deposition in mucous membranes or injured skin remain unknown.

Efficient elimination of *T. cruzi* is dependent on TNF-α, IL-12, IFN-γ and effector Th1 response [4, 5]. Early IFN-γ activates inducible nitric oxide synthase (iNOS) and nitric oxide (NO) production by MC with trypanocidal activity [6, 7]. INOS has also been involved in partial inhibition of T cells by myeloid-derived suppressor cells (MDSCs) [8, 9]. MDSCs are not fully differentiated cells released by the bone marrow (BM) and found in different pathological settings including cancer, autoimmunity and infections [9–11].While these cells share some similarities with granulocytes or inflammatory-monocytes (Mo), they can be highly suppressive by NO production, L-arginine depletion and regulatory T-cell (Treg cell) induction [9].

Myeloid cell heterogeneity has led to considerable confusion [12] since markers previously described for a particular group of cells are shared by different subsets. For example, in cancer the normal pathway of Mo differentiation towards dendritic cells (DCs) or MC can be altered [13], CD11c is expressed commonly by pulmonary MC [14], a subset of splenic MC are $CD11b^{low}$ [15], and F4/80 can be detected in DCs [16]. In addition, Mo can migrate to inflamed tissues [17, 18], and differentiate into professional antigen-presenting cells (APCs) [19]. In conclusion, not only the phenotype but the origin, the localization and the functionality define the myeloid cell type [20].

After skin infection APCs and phagocytes, including DCs, can reach the dermis and/or the dLNs [21]. Furthermore, under inflammatory conditions such as infections or injury, an additional subset of DCs differentiated from Mo, can be identified in local tissue or lymphoid organs [22].

Trypanosoma cruzi alters the immunogenicity of DCs in vitro [23, 24], and recently we have demonstrated that intradermal infection fuels immunoregulatory mechanisms involved in parasite persistence [25]. Nevertheless, the early events at *T. cruzi* portal of entry remain unknown.

Here, we describe a poor mobilization of leukocytes into the skin when injected with *T. cruzi*. However, the infection promoted rapid traffic of Mo to secondary lymphoid organs. Phenotypic-functional studies demonstrated that Mo-derived cells recruited into the spleen consisted in a heterogeneous population of Mo-derived cells including Mo-DCs. Mo-derived cell depletion by 5-FU confirmed their dual role during infection, limiting parasite multiplication by iNOS-dependent mechanisms and promoting *T. cruzi* persistence by impairing the development of an anti-parasite specific response.

Results

Low skin infiltrate after *T. cruzi* intradermal inoculation

The skin constitutes a complex network. While Langerhans cells (LCs) are the only APCs in epidermis, DCs, Mo and MC can be found in dermis [26].

After ear intradermal (id) inoculation of *T. cruzi*, there was no visible inflammation either soon or at 3 or 7 days post-infection (dpi) by macroscopic examination (Fig. 1A and Supporting Information Fig. 1A). At 72 h post-injection of Tp or PBS (not-infected controls, NI), microscopic analysis showed focal accumulation of cells in the skin of infected animals. Remarkably, only one to two fields out of 100 screened per slide showed cellular infiltrates between epidermis and dermis (infiltrated versus not-infiltrated skin, right and left panels; Fig. 1B). After skin enzymatic digestion, we found more $CD45^+CD11b^+$ leukocytes gated in R2 in Tp-inoculated ears compared to NI by flow cytometry (Fig. 1C).

When analysing the myeloid compartment in epidermis, most of the $CD11b^+$ cells co-expressed CD207, MHCII and $CD11c^{int}$, compatible with LCs, both in NI or infected animals (gate R3, Fig. 1D and Supporting Information Fig. 1B). However, an increasing percentage of $GR\text{-}1^+$ cells were detected in the epidermis of the Tp-injected ears particularly at 2 and 24 hours post-infection (hpi) (GR-1 versus CD11c panel, Fig. 1D). In addition to $GR\text{-}1^+$ cells, epidermis from Tp-injected mice showed two populations of $CD207^+$ cells with high or intermediate marker expression (CD11b versus CD207 panel, Fig. 1D). $CD11b^{high}CD207^{int}$ cells could constitute short-term LCs developed from Mo that repopulate the LC compartment [27]. Of note these cells presented low MHCII expression (CD11b versus MHCII panel, Fig. 1D).

Additionally in the dermis, more myeloid cells were also detected in infected than in control animals, including $GR\text{-}1^+$ (bottom, Fig. 1E) with enhanced expression of Ly6C and low levels of MHCII particularly at 24 hpi (upper and lower histograms, respectively; Fig. 1E), compatible with Mo.

In spite of the transient recruitment of myeloid cells into the skin, no amastigotes nests were detected until 7 dpi (data not shown), suggesting that *T. cruzi* seemed to pass almost unnoticed through the inoculation site. Cellular infiltrates were clearly detected in the auricular lymph node (LN), as previously described for popliteal LN after intradermoplantar inoculation of the parasite [25].

Early Mo mobilization to dLNs and changes in DC subsets

Mo recruitment into the skin and LNs followed by DCs differentiation at the site of infection has been previously reported for protozoan parasites such as *Leishmania major* and *Trypanosoma brucei* [21, 28].

After *T. cruzi* injection in hind feet or ears, popliteal and auricular dLNs presented swelling and enhanced cellularity (data not shown and Fig. 2A). By flow cytometry, we found that $CD11b^+$ cells infiltrated dLNs gradually, peaking at 8 dpi (Fig. 2B and C). The recruited population was negative for the granulocytic marker Ly6G, expressed $F4/80^{int}$, $Ly6C^{high}$ but low CCR2 compatible with Mo-derived cells (Fig. 2B and C, and data not shown). Strikingly, $Ly6C^+$ cells presented $CD115^{low}$ expression (Fig. 2D), in contrast to the blood-circulating counterpart (Supporting Information

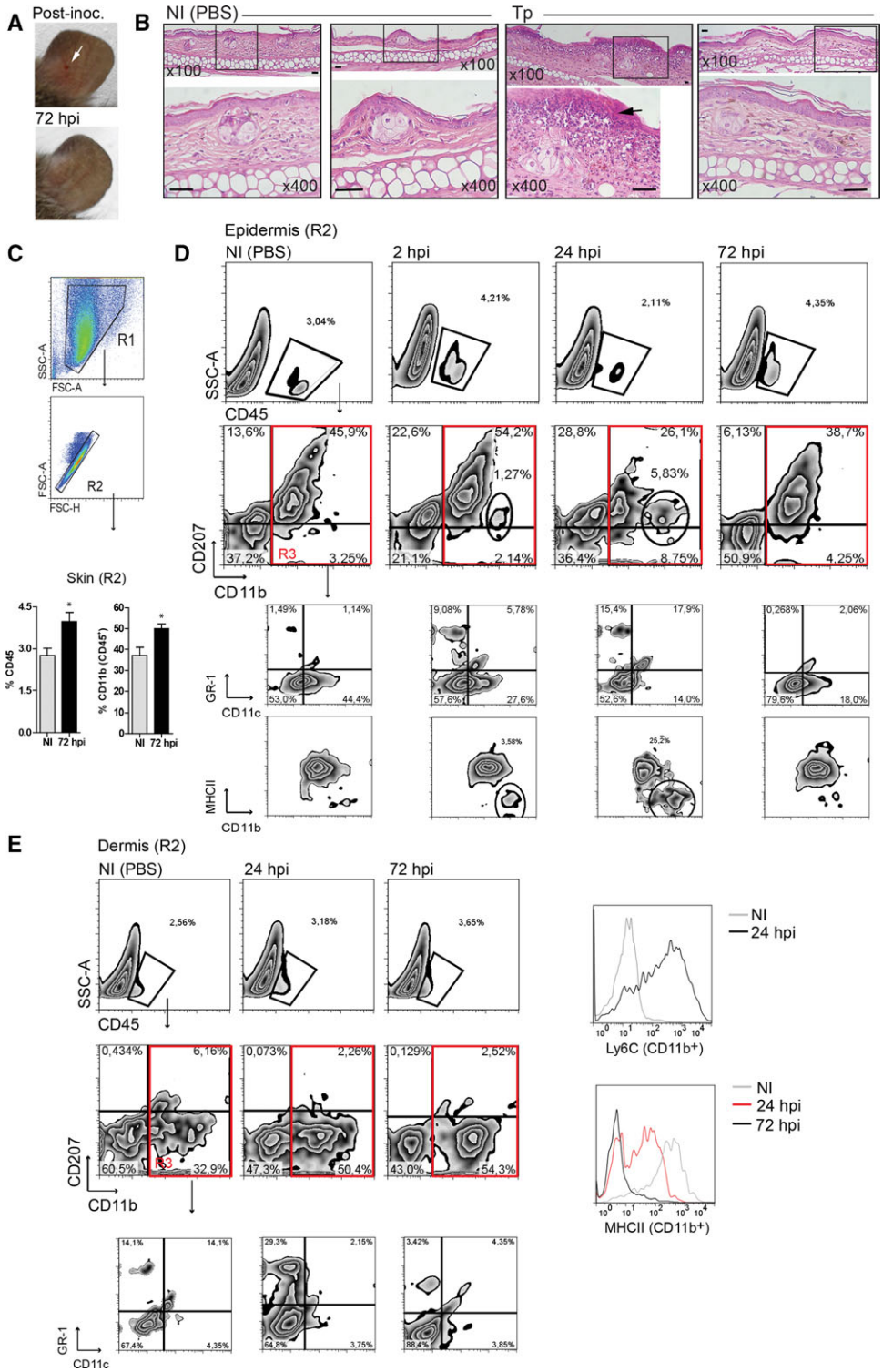

Figure 1. *T. cruzi* inoculated in the skin induces low and focal mobilization of leukocytes. C3H/HeN mice were intradermally (id) injected in ears with trypomastigotes (Tp) or PBS (NI). (A) Macroscopic examination of ears (white arrow shows the inoculation site). (B) Skin response was analysed by optic microscopy in samples stained with Hematoxylin and Eosin (black arrow, focal infiltrates between epidermis and dermis). Two representative images with two treatment conditions of six independent experiments are shown. Original magnification × 100 and × 400. Scale bars represent 20 μm. (C–E) Gating strategy for leukocytes ($CD45^+$) and myeloid cells ($CD11b^+$) detection in skin-cell suspension by flow cytometry at different times post-infection. (C) Percentage of $CD45^+CD11b^+$ in total skin cells at 72 h post-infection (hpi). Langerhans cells ($CD11b^+CD207^+$), DCs ($CD11c^+$), Mo and granulocyte ($GR\text{-}1^+$) quantification and analysis of the expression of MHCII in NI or at 2 (left), 24 (middle) and 72 (right) hpi in epidermis (D) and Langerhans cells, DCs, and Mo ($Ly6C^+$) identification in NI (left) and at 24 (middle) and 72 (right) hpi in dermis (E). Data are shown as mean + SEM of one experiment representative of five independent assays with two mice per group per assay. $^*p < 0.05$ (one tailed, unpaired Student´s *t*-test), compared to NI controls.

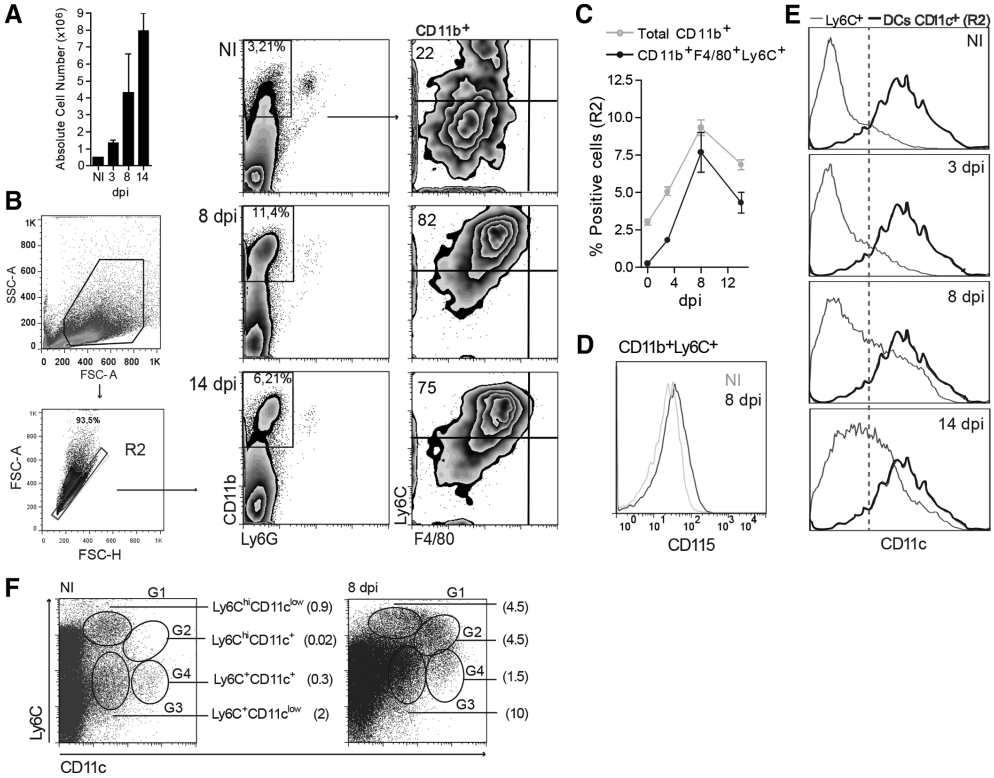

Figure 2. Ly6C$^+$ Mo recruitment into dLNs after intradermal *T. cruzi* inoculation. (A) Absolute cell number in popliteal LN (dLN) after Tp idp infection. (B-F) Gating strategy and characterization of the myeloid population in dLNs at different time points by flow cytometry. (B and C) Identification of myeloid population (CD11b$^+$); granulocytes (Ly6G$^+$) and Mo-derived cells (Ly6C$^+$F4/80$^+$) until 14 dpi. Data are presented as mean + SEM of five independent experiments. One representative experiment with two mice per sample is shown. Identification of (D) Mo (CD115$^+$) and (E) Mo-DCs (CD11c$^+$) in dLNs. (F) Characterization of Mo-derived cells by Ly6C and CD11c expression in R2. Gating strategy for Mo (G1), and Mo-derived cells (G2 and G4). One of five independent experiments with two mice per sample is shown.

Fig. 2), increased CD11c (Fig. 2E) and downregulated Ly6C expression (G1-G4, Fig. 2F).

Under steady state, at least five subsets of DCs have been described in LNs, and injury or infection can modify the repertoire. Migratory in contrast to resident DCs, express CD11c^{int} and MHCII^{high} under steady state but this changes during inflammation [16]. Here, Tp-injection incremented the number of CD11c$^+$ cells in dLNs, particularly the CD11b$^+$ subset (Fig. 3A). On the contrary, no increment was observed in CD11b$^-$CD11c$^+$, including the CD8α$^+$ classical (c)DCs, plasmocytoid and CD4$^-$CD8$^-$ double negative (DN) DCs until 8 dpi (Fig. 3A and data not shown). Remarkably, no migratory CD103$^+$ DCs were found and most of the CD11b$^+$ DCs displayed the Ly6C marker (Fig. 3B), resembling previously described iDCs [16, 29]. Strikingly, under the infection all DC populations described presented lower expression of MHCII than in the steady state, except for the Mo-derived iDC-like subset and CD8α$^+$ cDCs, the latter at 3 dpi (Fig. 3C).

Traffic of Ly6C$^+$Mo and enlarged CD11c$^+$ population in the spleen of infected mice

Mo can reconstitute tissue MC and DCs following trauma or infection [30, 31]. *Trypanosoma cruzi* infection incremented the absolute cell number in the spleen (Fig. 3D), and particularly the myeloid compartment (Fig. 3E). At 8 dpi, recruited cells were mostly granulocytic (Ly6G$^+$) or monocytic (Ly6C$^+$). The latter were sustained at least until 14 dpi (right panel, Fig. 3E) and more than a half of these cells co-expressed CD11c (P2, Fig. 3F).

We and others have previously reported myeloid cell recruitment into the spleen of *T. cruzi* infected mice [8, 25, 32]. Here we found that along the acute infection myeloid Ly6C^{high} and Ly6C$^+$CD11c$^+$ cells were particularly recruited into secondary lymphoid organs (Figs. 2D, 4A and B). However, only a small percentage of CCR2$^+$ inflammatory-Mo were detected in spleen at 8 dpi (Fig. 4C), but consistent with a migratory phenotype [33, 34], more than a half of the Ly6C$^+$CD11c$^+$ population expressed CD62L (G2, Fig. 4D).

Under steady state, Ly6C$^+$ Mo population in the spleen was small (G1) and Ly6C$^+$CD11c$^+$ cells (G2) were practically absent (Fig. 4B). During infection, Mo-derived cells that reached the spleen lost CD115 (Fig. 4E), downregulated Ly6C and gained CD11c (Fig. 4B and E), MHCII and CD86 expression, resembling previously described Mo-derived/iDCs [31]. Cells gated in G1 and G2 upregulated CD64, consistent with activated Mo and Mo-derived cells (Fig. 4E). Furthermore F4/80$^+$MerTK$^+$ Mo-derived MC, normally associated to wound repair, were also detected at 14 dpi (G3, Fig. 4E).

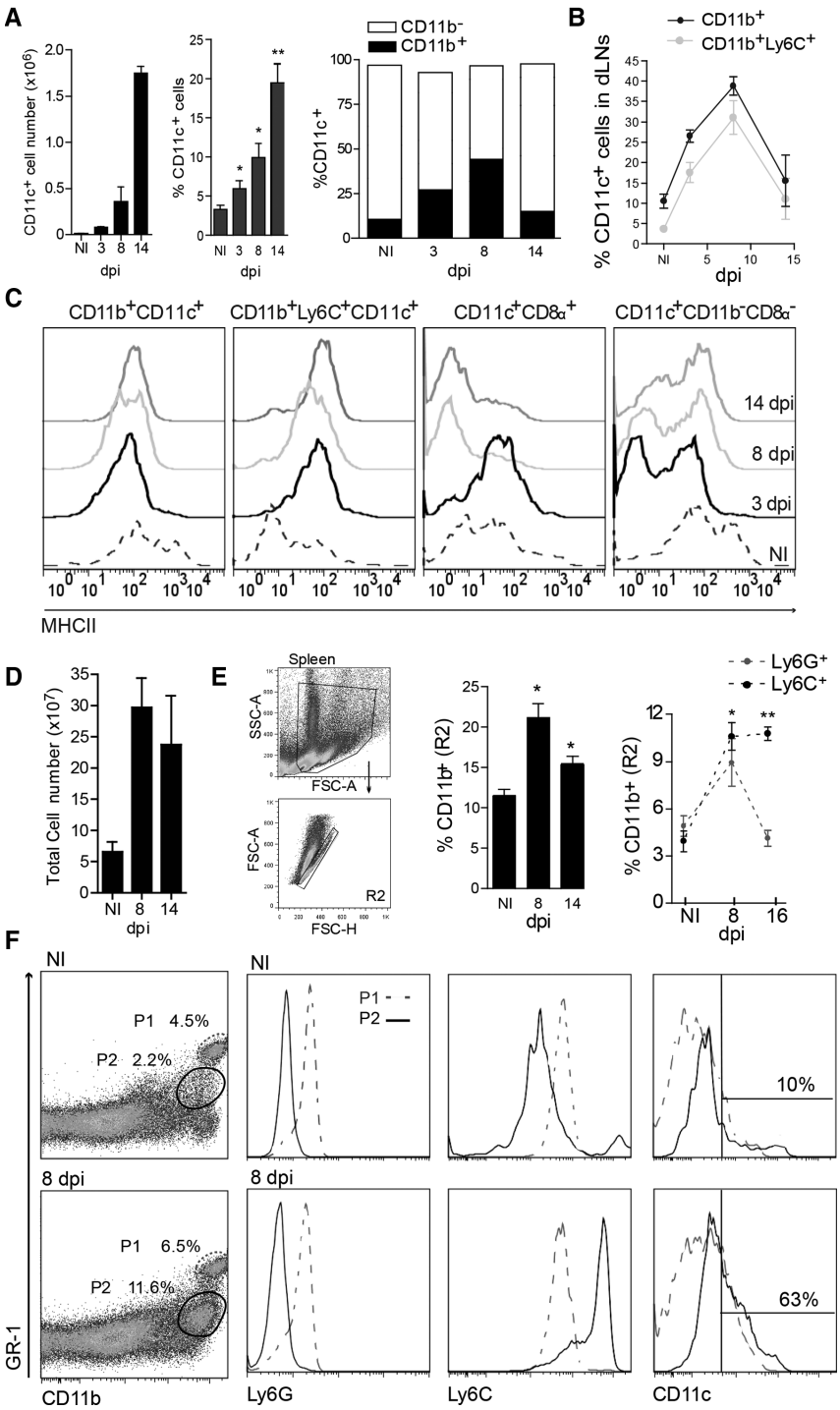

Figure 3. Mo-DCs mobilization to secondary lymphoid organs in infected mice. (A-C) Identification of $CD11c^+$ DCs in dLNs after idp injection of Tp by flow cytometry. (A) Absolute DC number (left panel), percentage (middle) and proportion of myeloid and non-myeloid DCs (right). $^*p < 0.05$, $^{**}p < 0.01$ (one-way ANOVA and Bonferroni´s post-test), compared to NI controls. (B) Kinetics of total myeloid and $Ly6C^+$ DCs in dLNs during acute infection. Data are represented as the mean + SEM of five independent experiments with two mice per group per experiment. (C) Expression of MHCII in $CD11b^+$ cDCs, $Ly6C^+$ Mo-DCs, $CD8\alpha^+$ cDCs and $CD11b^-CD8\alpha^-$ subsets (including $CD8^-CD4^-$ DN DCs and pDCs). One representative experiment of five independent assays with two mice per experiment is shown. (D–F) Characterization of myeloid cells in spleen during infection. (D) Absolute cell number of splenocytes expressed as the mean + SEM of five independent experiments. (E) Gating strategy for the identification of myeloid cells in spleens (left-middle panels) and kinetics of granulocyte ($Ly6G^+$) and $Ly6C^+$ Mo-derived cells (right) during the acute infection. Mean + SEM of five independent experiments with two mice per group. $^*p < 0.05$, $^{**}p < 0.01$ (one-way ANOVA and Tukey´s post-test), compared to NI controls. (F) Granulocyte (Ly6G), Mo (Ly6C) and DCs (CD11c) identification in two $GR\text{-}1^+$ myeloid populations (P1 and P2) in NI mice or at 8 dpi. One representative result of five independent experiments pooled from two mice per group per experiment is shown.

$Ly6C^{high}$ Mo recirculate to the BM in the absence of inflammation [17, 35], and undifferentiated can be found in tissues such as blood, LNs or spleen [34]. To confirm the origin of iDC-like found in the spleen of *T. cruzi*-infected mice, $Ly6C^+$ Mo were purified by cell-sorting from the BM of *CD11c-GFP* animals and then, adoptively transferred into NI or 3 day-infected mice (Supporting Information Fig. 3A). Since the $Ly6C^+CD115^+$ population can be heterogeneous and include $Flt3^+CD11c^+$ pre-DCs [36], we purified and adoptively transferred the $CD11b^+Ly6C^{high}CD115^+Ly6G^-CD11c\,GFP^-$ population to avoid the transfer of immature DCs (Supporting Information Fig. 3B). At day 4 post cell transfer, spleens from NI or infected animals were harvested and analysed to detect GFP^+ Mo-DCs. We observed the traffic of $CD11cGFP^+$ cells only in the spleen of infected animals (Fig. 4F). These cells displayed CD11c and also Ly6C expression, confirming their monocytic origin (Fig. 4G). In addition, while *Zbtb46* expression was absent in $Ly6C^{high}$ sorted-Mo, the transcription factor was slightly upregulated in

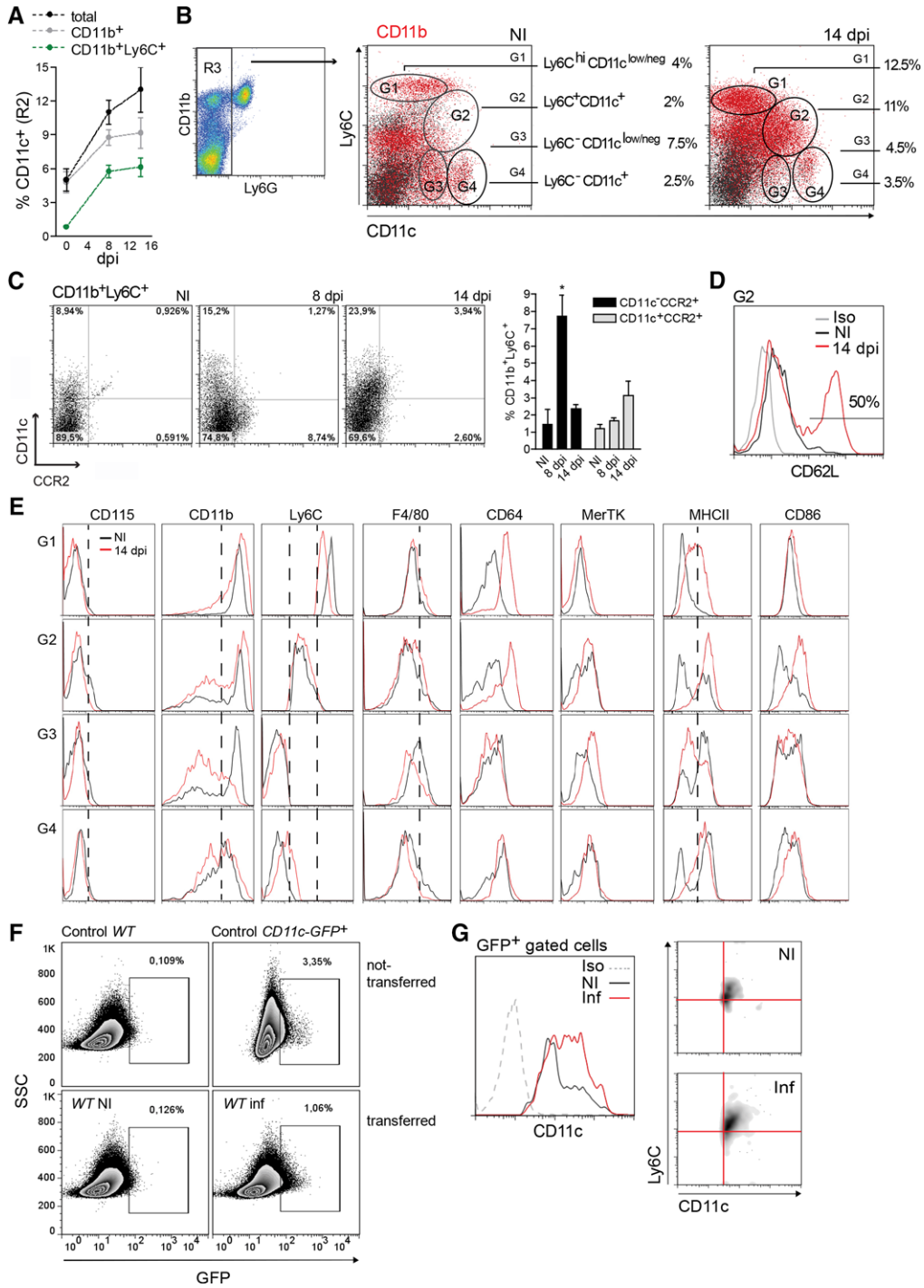

Figure 4. *T. cruzi* infection promotes the traffic of Mo-DCs into the spleen. (A) Kinetics of total, myeloid and Mo-DCs in R2 gated splenocytes (as shown in Fig 3). Mean + SEM of seven independent experiments and pooled from two mice per experiment. (B) CD11c expression in $CD11b^+Ly6C^+$ cells in R3 (excluding $Ly6G^+$ granulocytes) and quantified by flow cytometry. Representative results of five independent experiments with two mice per group are shown. (C) CCR2 and (D) CD62L expression in $CD11b^+Ly6C^+$ populations from the spleens of NI, 8 and 14 day-infected animals. One dataset representative of three independent experiments with two mice per group per experiment is shown. (E) Phenotypic marker expression in G1-G4 subpopulations from the spleens of NI (black histograms) or infected (14 dpi, red histograms) mice. One dataset representative of seven independent experiments with one mouse per experiment is shown. (F-G) BM-Mo adoptive transfer experiments. (F) Expression of GFP in splenocytes from negative (WT) and positive (*CD11c-GFP*) control mice (upper panels), and from NI or 3-day infected WT recipient mice adoptively-transferred with BM-Mo from *CD11c-GFP* transgenic donors (lower panels), (see also Supporting Information Fig. 3). The frequency of $CD11cGFP^+$ cells was determined by flow cytometry. (G) Flow cytometric analysis of GFP^+ gated cells from NI (black line and top) and infected (red line and bottom) transferred-mice by CD11c and Ly6C staining. (F and G) One representative experiment of three independent assays with similar results performed with two mice per group is shown.

CD11cGFP$^+$ cells obtained from the transferred-infected-animals (Supporting Information Fig. 3C), confirming Mo commitment to DC during infection [36, 37].

Reduced capacity to induce ex vivo lymphoproliferation in splenic Mo-derived cells from infected mice

Inflammatory-Mo and Mo-DCs have been described in the context of several infections [17, 38]. Both can display TNF-α, iNOS activation and access to T cell areas [32]. Mo does not express CD11c, MHCII and CD86 [18, 19, 31, 39], however adoptively transferred cells can differentiate into DCs that progressively lose Ly6C and acquire MHCII during inflammation [40].

Hence, we proceeded to better characterise in vitro the functional properties of CD11b$^+$Ly6C$^+$Ly6G$^-$ cells recruited into the spleen of infected animals. More than 50% of the sorted cells displayed CD11c^{int} (Fig. 5A). Zinc finger transcription factor ZBTB46 is expressed in cDCs and not in Mo or other immune cells [41]. However, it was recently shown that Ly6C^{high} Mo can differentiate into ZBTB46$^+$ Mo-DCs [37]. Previous studies reported the dispensable role of GM-CSF in the development of Mo-DCs in inflamed tissues [42], but it was later confirmed that the differentiation of fully-functional Mo-DCs from Mo is optimal in response of GM-CSF and IL-4 [36, 37]. Here, we observed no Zbtb46 in Ly6C$^+$ Mo, but a low expression in the CD11b$^+$Ly6C$^+$CD11c$^+$ subset in comparison with myeloid cDCs, confirming Mo-DCs differentiation from Mo (Fig. 5B). Ex vivo, Ly6C$^+$ sorted-cells cultured alone or with GM-CSF showed little change in Ly6C and CD11c marker expression, but enhanced cell dead (Fig. 5C and D).

NO is one of many mediators involved in inflammation, and it can be immunosuppressive when being produced by MDSCs [9]. The activation of immunomodulatory mechanisms, including NO production by MDSCs, has been described for *T. cruzi* infection [8, 11, 43]. Ly6C$^+$ cells from infected animals produced nitrite that was reduced in cultures with GM-CSF (Fig. 5E). TNF-α and IL-10 were also found in culture supernatants and while no difference in TNF-α production was detected, less IL-10 was secreted in the presence of GM-CSF (Fig. 5F).

Next, we analysed the capacity of Mo-derived cells to induce T-cell proliferation. As expected, Mo from naïve mice and Mo-derived cells from the infected mice did not stimulate T cells as cDCs, and measured by Ki-67 expression (Fig. 5G). However, when CD11c$^+$ cells were depleted from the Ly6C$^+$ population (Ly6C$^+$CD11c$^-$), T cells displayed enhanced proliferation measured by CFSE dilution (Fig. 5H), suggesting population functional heterogeneity.

Consistently incubation with aminoguanidine (AG), a selective inhibitor of iNOS, reduced nitrite concentration detected in cultures of CD3$^+$ T cells with total Ly6C$^+$ (Fig. 5I). Although treatment with AG did not restore T-cell proliferation in these cultures (data not shown), as previously described for splenocytes from iNOS deficient mice [8], it boosted IFN-γ secretion independently of Ly6C$^+$ cell identity. Moreover, AG reduced IL-10 levels in cultures of T cells with total Ly6C$^+$ cells (Fig. 5I). These results confirmed the heterogeneous nature of Mo-derived cells, and suggested an immunosuppressive role for Mo-DCs.

Mo-derived cells control parasite clearance but impair T-cell activation

5-fluorouracil (5-FU) is a chemotherapeutic drug described to mediate myeloablation by reduction of Mo in mice [44]. In addition, it was reported to induce anti-tumour response by selectively depleting myeloid suppressor cells without affecting other cell types [45]. To study the role of Mo-derived cells in vivo, mice were treated with 5-FU on day 3 post-infection and the effect was followed over the course of the infection. 5-FU reduced spleen size (data not shown), and splenocyte cell-counts in infected mice (Fig. 6A). As previously reported, splenic B cells, T cells, DCs, total myeloid cells, Mo and granulocytes were not affected by 5-FU in NI mice (Fig. 6B, C and Supporting Information Fig. 4A). However, 5-FU severely reduced the number of CD11b$^+$ cells during infection (R3, Fig. 6B), in accordance with a previous report [11]. Strikingly, 5-FU treatment partially restored *Zbtb46* expression in the spleen, which was severely affected during infection (Fig. 6C). This effect was accompanied by a reduction in the Ly6C$^+$ population from the BM and blood (Supporting Information Fig. 5A) and with the loss of a discrete subpopulation of Ly6C$^+$CCR2$^+$ inflammatory-Mo from the circulation (Supporting Information Fig. 5B).

Mo-derived cells depletion by 5-FU (Fig. 6D), affected TNF-α and IFN-γ production by splenocytes (Fig 6E), the latter not from T-cell source (Fig. 6F). Consistently, 5-FU downregulated iNOS mRNA, protein expression (Fig. 6G) and NO production (Fig. 6H) in the spleen of infected mice. To test the effect of Mo-derived cell depletion in the outcome of the infection, we analysed parasitemia and mortality in treated and control mice, after confirming no side effects of 5-FU in parasite survival and multiplication in vitro (Supporting Information Fig. 4B and C). Myeloablation by 5-FU led to an increased parasitemia and high mortality beyond the acute phase of the infection (Fig. 6I). This could be explained by the downregulation of IFN-γ and NO, both critical for parasite-killing [7]. Ex vivo culture of splenocytes from 5-FU treated mice displayed a high number of free parasites (Fig. 6J), and more infected MC compared with untreated, confirming the importance of Mo-derived cells in the control of early *T. cruzi* dissemination during infection.

In vitro/ex vivo results suggested a suppressor property for the recruited cells, especially the Mo-DCs. In vivo, the elimination of Mo-derived cells highlighted their critical role in the control of the parasite load during the acute infection. Nevertheless, treatment with 5-FU induced enhanced T-cell response, detectable at 40 dpi during the chronic infection (Supporting Information Fig. 5C). The differences in T-cell subsets found between infected animals treated or not with 5-FU (Fig. 6K), were independent of Tregs (Supporting Information Fig. 5D), and could be explained by the shift in the proportion of cDCs versus Mo-DCs. Although

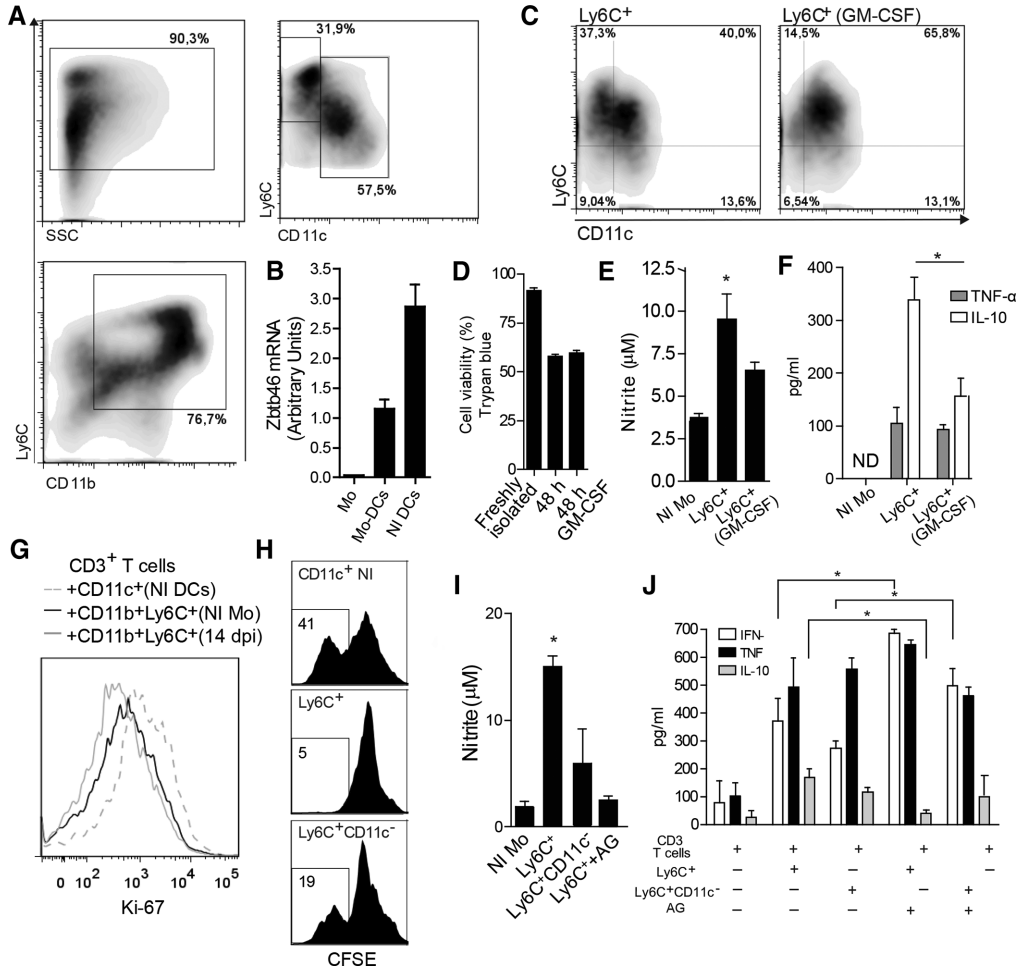

Figure 5. Ex vivo characterization of Mo-derived cells from *T. cruzi* infected mice. Phenotypic and functional characterization of Mo-derived cells purified from spleen by cell-sorting. (A) CD11b, Ly6C and CD11c expression. (B) *Zbtb46* transcript levels in Mo ($CD11b^+Ly6c^{high}$), Mo-DCs ($CD11b^+Ly6C^+CD11c^+$) and control $CD11b^+$ DCs from spleen of infected animals by RT qPCR and normalize to *GAPDH*. Means + SEM from three independent experiment set in triplicates are shown. (C) Ly6C and CD11c expression after 48 h culture with (right panel) or without (left panel) GM-CSF. One representative dataset of three independent experiments with samples pooled from two mice per experiment is shown. (D) Cell viability in freshly prepared samples or 48 h cultures with or without GM-CSF. (E) Nitrite detection in culture supernatants with or without GM-CSF (mean + SEM, of three independent experiment with samples set in triplicates), $^*p < 0.05$ (one-way ANOVA and Tukey´s post-test), compared to NI Mo. (F) TNF-α and IL-10 detection in cultured supernatants with or without GM-CSF by ELISA. ND: not detected, $^*p < 0.05$ (one tailed, unpaired Student´s t-test). (G) Expression of Ki-67 in T cells ($CD3^+$) cultured with Mo-derived cells or NI DCs and T-cell proliferation (H) measured by CFSE dilution in anti-CD3 plate-bounded assay by flow cytometry. Data are representative of three independent experiments with similar results consisting of samples from two mice in each independent experiment. (I) Nitrite detection in culture supernatants from T cells with NI Mo and total or CD11c-depleted $Ly6C^+$ cells from the spleens of infected mice (8 dpi). AG: aminoguanidine. Data are presented as mean + SEM from three independent experiments with two mice per group, $^*p < 0.05$ (one-way ANOVA and Tukey´s post-test), compared to NI Mo. (J) IFN-γ, TNF-α and IL-10 detection in culture supernatants from (I) by ELISA. Data are shown as mean + SEM of three independent experiments with two samples per experiment, $^*p < 0.05$ (one-way ANOVA and Tukey´s post-test).

no specific IFN-γ^+CD4^+ T cells were detected in the spleen until the chronic infection, a higher number was found in mice that received the myeloablation (Fig. 6L). These results demonstrate that immunosuppression exceeds the presence of Mo-derived cells.

In conclusion, we confirmed that myeloid cells recruited to secondary lymphoid organs during *T. cruzi* acute infection consist of a heterogeneous population of Mo-derived cells that include Mo-DCs. In addition, we demonstrated a dual role for these cells, controlling parasite multiplication and interfering with the development of a specific anti-parasite response.

Discussion

In the present study, we identify a population of myeloid cells consisting in a heterogeneous group of Mo-derived cells that infiltrate LNs and spleen, early after *T. cruzi* infection. We demonstrate that Mo-derived cells gradually differentiate into Mo-DCs and display a dual role in parasite control.

Previous reports demonstrated the importance of IFN-γ and NO to resist *T. cruzi* acute infection [7]. However, it was also described the presence of MDSCs and the activation of immunomodulatory mechanisms in order to counteract inflammation [8], not only in

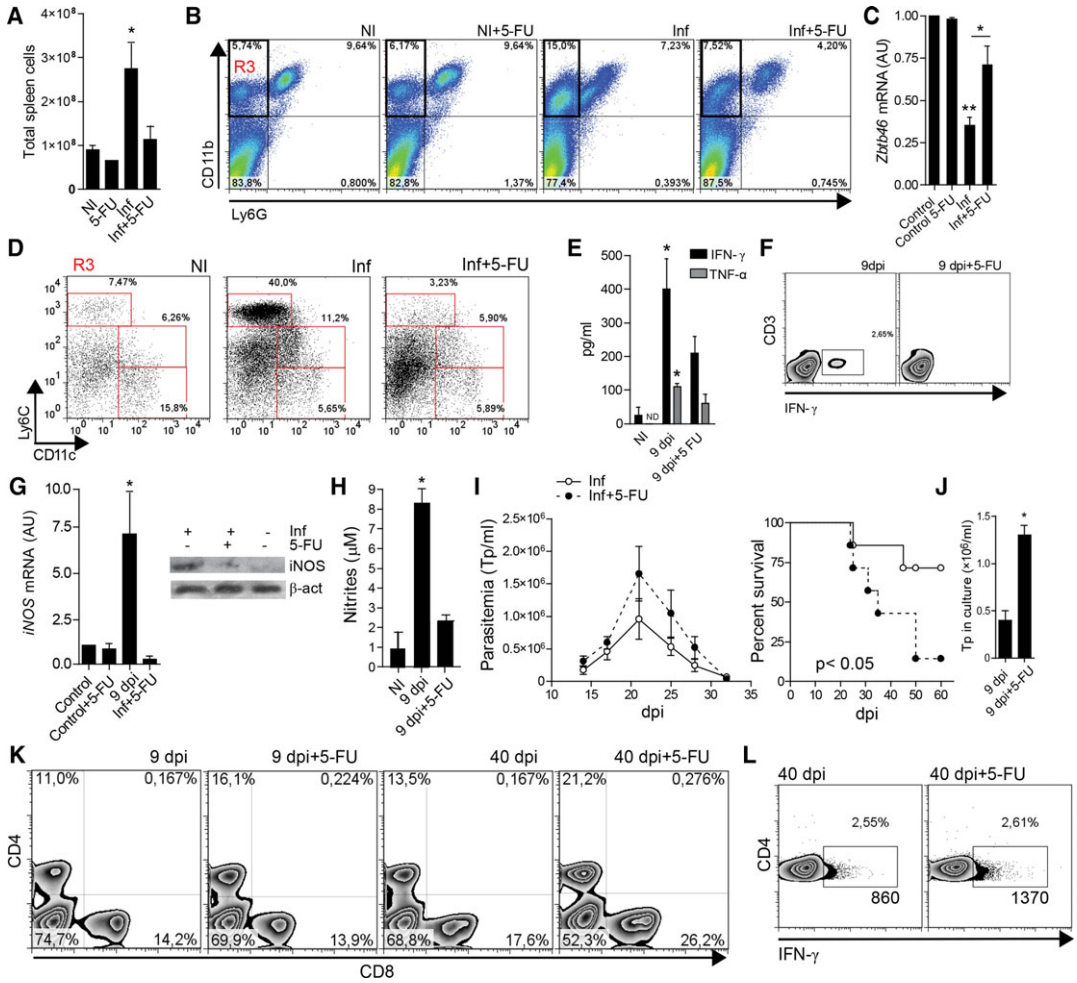

Figure 6. Depletion of Mo-DCs by 5-FU impairs parasite clearance but enhances T-cell response. Characterization of the effect of 5-FU in spleen. (A) Absolute cell number in NI or in 5-day infected mice as described in materials and methods. Data are expressed as mean + SEM from three independent experiments with two mice per group. $^{*}p < 0.05$ (ANOVA and Tukey´s post-test). (B) Ly6G^{-} and Ly6G^{+} myeloid cells in R2 as described in Fig. 3E above. Representative density plots of three independent experiments with two mice per sample per experiment are shown. (C) *Zbtb46* transcript levels in splenocytes were determined by RT qPCR and normalized to GAPDH. Means + SEM from three independent experiment set in triplicates are shown. $^{*}p < 0.05$, $^{**}p < 0.01$ (one-way ANOVA and Tukey´s post-test), compared to NI or between treatments. (D) Ly6C and CD11c expression in CD11b^{+}Ly6G^{-} cells gated in R3 from (B) above. (E) TNF-α and IFN-γ detection in culture supernatants from splenocytes by ELISA. ND: not detected. $^{*}p < 0.05$ (one tailed, unpaired Student's t-test), 9 dpi compared with 9 dpi+5-FU. (F) Intracellular IFN-γ in splenocytes from infected (left) and infected and 5-FU treated (right) by flow cytometry. One result from three independent experiments with two samples per experiment is shown. (G) *iNOS* transcript level in splenocytes was determined by RT qPCR and normalized to GAPDH (mean + SEM, left) and iNOS protein detection by immunoblot, β-actin was measured as loading control (right). Data are representative of three independent experiments. $^{*}p < 0.05$ (one-way ANOVA and Tukey´s post-test), compared to NI. (H) Nitrite detection in splenocyte culture supernatants from infected mice treated or not with 5-FU and NI controls (48 h). Means + SEM obtained from three independent experiments with two samples per experiment are shown. $^{*}p < 0.05$ (one-way ANOVA and Tukey´s post-test), compared with NI. (I) Peripheral blood parasitemia, and mice survival was monitored during infection. One representative experiment of three performed with five to seven mice per group is shown. Parasitemia is expressed as mean + SEM. $^{*}p < 0.05$ (unpaired Student's t-test and Kaplan-Meier, respectively). (J) Number of free Tp in splenocyte culture supernatants from infected mice treated or not with 5-FU (Mean + SEM, $n = 3$). $^{*}p < 0.05$ (one tailed, unpaired Student's t-test). (K) Splenic CD4^{+} and CD8^{+} T cells during the acute (9 dpi) or the chronic (40 dpi) infection with or without 5-FU treatment. One representative experiment of three with two mice per group is shown. (L) Relative number of antigen-specific IFN-γ^{+}CD4^{+} T cells 40 dpi in mice treated or not with 5-FU. Intracellular detection of IFN-γ was performed by flow cytometry. Plots are representative of three independent experiments with two mice per group.

the context of acute myocarditis [43], but also in liver inflammation [11]. Accordingly, here we describe the rapid appearance of myelomonocytic cells and their traffic to dLNs and spleen after Tp-injection into the skin.

The proper identification of Mo-derived cells, including DCs, macrophages, and MDSCs on functional basis in vivo, is a hard task [20]. Given the classification proposed by Guilliams and colleagues, we could identify the cells described here as 'suppressor MCs' since in general they functionally resembled MDSCs.

Inflammatory-Mo are central for pathogen clearance, on the contrary MDSCs can prevent pathogenic side effects in inflammation. Both, microenvironment and pathogens can condition myeloid cell plasticity. The occurrence of inflammatory-Mo and Mo-derived cells, including MDSCs and Mo-DCs, was confirmed

under pathological settings. Regarding Mo-DCs and MDSCs, while it is proposed that both share a common origin [46], they can be functionally opposite [9, 21]. However, assays conducted in vitro are not always representative for the in vivo facts. For example, in a model of sepsis MDSCs can be inflammatory and harmful early, while suppressive and protective against immunoreactivity in a late phase of the infection. Only initially, authors found an enhanced number of inflammatory cells with intermediate expression of CD11c, in addition to production of TNF-α and NO [47]. In the present work, we show that *T. cruzi* triggers the recruitment of Mo-derived cells that gained CD11c marker during the course of the infection. These cells produced IL-10, TNF-α and NO ex vivo and in vivo and displayed low capacity to induce T-cell response. In *Leishmania major* infection, Mo-DCs recruited into the inflamed skin are infected and transport antigens to T-cell areas [48]. On the contrary and similar to our findings, in *Plasmodium chabaudi* infection a population of $Ly6C^{+}CD11c^{low}$ cells described as Mo that presented TNF-α production and iNOS activity, were responsible for the clearance of the parasite and displayed poor antigen-presenting capacity [39]. During *T. brucei* infection, Mo recruitment into the liver and their differentiation in to $TNF\text{-}\alpha^{+}iNOS^{+}$ iDC-like resulted in detrimental inflammatory pathology with no changes in parasitemia [38].

Recent reports, based on the study of transcriptional profiles, confirmed the heterogeneity of $Ly6C^{+}$ Mo and the checkpoints involved in the differentiation of MC versus Mo-DC under steady state [36], in addition to the programs controlling cross-priming in cDCs and Mo-DCs [37]. Pathological conditions could add complexity to the scene. Supported by our observations, the phenotypic and functional heterogeneity observed in Mo-derived cells brings to light the fact that under infection, the fate of Mo-derived cells takes place outside the BM. This fuels the idea that both Mo-DCs and those resembling M-MDSCs during *T. cruzi* infection could be two sides of the same coin.

Previous work from our group demonstrated that *T. cruzi* impairs immunity via endogenous mechanisms by fostering the tolerogenic dialog between DCs and other cell types [24, 25, 32]. Here we described that *T. cruzi* is able to silently access through mouse skin. However, early after infection the parasite induces the recruitment of Mo-derived cells to secondary lymphoid organs. The ablation of Mo-derived cells and their differentiation into Mo-DCs confirmed the contribution of these cells in parasite killing by iNOS-dependent mechanisms and, in agreement with previous results, their negative influence in the development of an anti-parasite effector response. Given Mo-derived cells heterogeneity, further advances in the field will enable a better classification of these cells and their use as targets for therapy.

Materials and methods

Mice, infection

B6.FVB-Tg (Itgax-DTR/EGFP) 57Lan/J transgenic and *wild type* mice, referred as *CD11c-GFP* and WT respectively, were purchased from The Jackson Laboratory (Bar Harbor, ME). C57BL/6 WT or *CD11c-GFP* and C3H/HeN mice were maintained in the animal facilities of IMPaM UBA-CONICET, Facultad de Medicina, Universidad de Buenos Aires, and bred under sanitary barrier in specific-pathogen-free conditions. Eight-to-ten week old male mice were injected with 500 blood-purified Tp from RA strain in the ear or the hindfoot. Parasite load and mortality were daily recorded [25].

All experiments were performed according to protocols CD N° 04/2015 approved by the University of Buenos Aires´s Institutional Committee for the Care and Use of Laboratory Animals (CICUAL) in accordance with the Council for International Organizations of Medical Sciences (CIOMS) and International Council for Laboratory Animal Science (ICLAS) international ethical guidelines for biomedical research involving animals.

Antibodies and cell sorting reagents

The following monoclonal antibodies (Abs) were used: isotype controls, anti-CD11b and anti-CD45.2 (APC, M1/70 and ALI-4A2; Ligatis Biotech Argentina), anti-CD103 (FITC, M290), anti-Gr-1 (FITC, RB6-8C5), anti-CD11b (APC, M1/70), anti-CD4 (FITC, L3T4), anti-CD8 (APC, Ly-2), anti-CD3 (PerCP, 145-2C11), anti-CD62L (PE, MEL-14), all from BD Biosciences; anti-MHC II (PE-Cy5, M5/114.15.2) from eBioscience; anti-Ly6G (FITC, 1A8), anti-MHCII (FITC, M5/114.15.2), anti-CD115 (biotin, AFS98), anti-CD207 (PE-Vio770, caa8-28H10), anti-CD11c (PE, N418), anti-CD11b (APC, M1/70.15.11.5), anti-Ly6C (PE-Vio770, 1G7.G10), anti-CD4 (FITC, GK1.5), anti-CD8a (PerCP, 53–6.7), anti-CD3 (biotin, 145-2C11), anti-CCR2 (biotin, REA538) and anti MerTK (biotin, REA477) all from Miltenyi Biotec. Anti-F4/80 (biotin or FITC, BM8), and anti-CD64 (PE, X54-5/7.1) were from BioLegend. Secondary reagents: FITC, PE, Cy5 or PE-Cy7 streptavidin, isotype controls and anti-IFN-γ (Alexa Fluor®647, XMG1.2) were from BD Biosciences and Treg cell detection kit and CD11c MicroBeads, PE or streptavidin MicroBeads for cell magnetic sorting all from Miltenyi Biotec.

Histological analysis

Ears from Tp-injected (3 dpi) and PBS-injected (NI) animals were fixed and preserved in 10% (v/v) formalin and then embedded in paraffin. Sections of 50 μm in thickness were stained with hematoxylin and eosin. Infiltrated skin was identified after microscopic observation of at least 20 fields per section (5 sections per ear and slide, and set in triplicate) by Nikon Eclipse E200 or a Primovert ZEISS light microscope (× 100- × 400).

Cell sample

Epidermal sheets were obtained from the skin of ears by using trypsin (1% and 0.3%; Sigma), as previously described [49]. Cell suspensions from dermis or epidermis tissue were obtained by

mechanically and/or enzymatically disaggregation using collagenase D and DNase I (1 mg/mL and 20 μg/mL, respectively; Sigma-Aldrich) at 37°C for 30 min. Spleens were treated with hyaluronidase IV-S (200 U/mL; Sigma-Aldrich) and collagenase II (250 U/mL; Invitrogen), mechanically disaggregated and passed through a 100 μm nylon mesh (BD, Bioscience).

After tissues homogenization, red blood cells were lysed by Tris 0.83% ammonium chloride buffer (pH 7.2), and viability determined by Trypan blue exclusion. Mo from BM, splenic Mo-DCs or dLNs T cells were isolated by FACSAria cell sorter or using magnetic selection (MiniMACS; Miltenyi Biotec), as previously described [25]. Purification was > 90%.

Flow cytometry

Flow cytometry analysis from skin, BM, dLNs, blood and spleen cell suspensions were performed after quadruple/quintuple staining by the gating strategies indicated in figures. For surface staining, cell suspensions were incubated with fluorescence-labeled mAb for 30 min at 4°C. For specific IFN-γ detection in $CD4^+$ and $CD8^+$ T cells, cell were cultured in the presence of *T.cruzi*-Ag (20 μg/mL) together with brefeldin A (10 μg/mL; Sigma-Aldrich) for 5 h previous surface staining. Then cells were fixed and permeabilized with Cytofix/Cytoperm (BD Biosciences) [25]. Sample acquisition was achieved on FACSCanto or FACSAria flow cytometers (BD Biosciences) and analysed by FlowJo 7.6 software.

Adoptive transfer experiments

For Mo transfer, donors were *CD11c-GFP* mice and recipient infected or NI WT mice. Briefly, 2×10^6 $CD11b^+Ly6C^{hi}CD115^+Ly6G^-CD11cGFP^-$ Mo sorted from BM were transferred intravenously into infected (3 dpi) or NI mice. After 4 days, $CD11b^+Ly6C^+Ly6G^-CD11cGFP^+$ cells were detected in spleens (Supporting Information Fig. 3) and purified for RNA extraction.

RT qPCR and end-point PCR

RNA purification from Trizol (Invitrogen) and cDNA synthesis were performed as previously described [25]. Quantitative PCR was performed by using EvaGreen qPCR Mix Plus (Solis BioDyne). Primers: *Zbtb46*, 5′-TCA CAT ACT GGA GAG CGG C-3′ (F) and 5′-CCT CAT CCT CAT CCT CAA CC-3′ (R); *iNOS*, 5′-CAG AGC AAT ATA GGC TCA TCC A-3′(F) and 5′-GGA TTT CAG CCT CAT GGT AAA C-3′(R) and *GAPDH*, 5′-CCA GAA CAT CAT CCC TGC AT-3′(F) and 5′-GTT CAG CTC TGG GAT GAC CTT-3′(R); qPCR was set in a StepOne Plus™ (Thermo Fisher Scientific). Results were normalized to *GAPDH* expression (reference) and expressed as mRNA arbitrary units (AU).

Cell-functional assays

T-cell proliferation was analysed by CFSE dilution in $CD3^+$ T cells stimulated with and without total $Ly6C^+$ or $Ly6C^+CD11c^-$ (1:5 ratio) in plate bound anti-CD3 for 72 h or by Ki-67 detection as previously described [25].

For TNF-α and IL-10 detection by ELISA (R&D Systems), cell culture supernatants were stored at -80°C until used according to manufacturer's protocol.

Nitrite detection

NO production was determined by nitrite detection by Griess reaction. Briefly, cells were cultured for 48 h; supernatants collected and treated with 1% sulfanilamide and 0.1%N-naphtylethylenediamine hydrocloride in 2.5% H3PO4 for 5 min at room temperature in the dark. Then, absorbance was measured at 540 nm, and concentrations were extrapolated from a sodium nitrite standard curve.

Immunoblot

Splenocytes were washed, treated with ice-cold lysis buffer (20 mM Tris-acetate, pH 7.0, 1 mM EGTA, 1% Triton X-100, 0.1 mM sodium fluoride, 5 μg/mL leupeptin, 1 mM sodium orthovanadate, 1 mM phenylmethylsulfonyl fluoride) and stored at -20°C until use. For immunoblot, equal amounts of protein (30 μg) were resolved by SDS-PAGE and probed with anti-iNOS polyclonal Ab (Santa Cruz Biotech) or anti-β-actin Ab (Abcam Inc.) followed by HRP-conjugated anti-rabbit or mouse IgG secondary Ab (Santa Cruz Biotech) and detected by enhanced chemoluminiscence (ECL; GE Healthcare) according to manufacturer's instructions.

5-FU treatment

For myeloablation, NI or 3-day-infected C3H/HeN mice received a single intraperitoneal injection of 5-FU (50 mg/kg; Microsules Argentina). Untreated controls received PBS injection. Spleens were harvest and cells obtained at 5, 9 or 40 dpi.

To test 5-FU effect on parasite viability or multiplication, free parasites or Vero monolayers with Tp (1:1, cell:Tp ratio) were cultured in 5 mg/mL and 1/10 serial dilutions of 5-FU in RPMI-1680 medium supplemented with 5% of heat-inactivated FCS (Internegocios, Argentina) ON. Then parasites were removed and cells cultured for 5 days. Monolayers were stained with Giemsa and infection analysed by microscopic examination (× 100).

Statistical analysis

Statistical significance was determined by Student's *t*-test, ANOVA and Tukey´s or Bonferroni´s post-test. P value <0.05 was

considered significant and analysed by using GraphPad Prism 5 software for Windows.

Acknowledgements: We thank Dra. Marisa Gómez (University of Buenos Aires, Argentina), for the 5-fluorouracil supply, Dra. Marcela Cucher (University of Buenos Aires, Argentina) for the critical reading of the manuscript and Dra. Juliana Idoyaga (Stanford University, United States) for advice and technical support. This study was supported by *Fundación Bunge y Born*, *Subsidio para la Investigación en la Enfermedad de Chagas* (C.V.P.) and CONICET PIP112-201101-00913 (S.M.G.C). C.V.P. designed and performed all experiments, analysed data, wrote and edited the manuscript. S.M.G.C supervised the editing and the writing of the manuscript.

Conflict of interest: The authors declare no commercial or financial conflicts of interest.

References

1 **Padilla, A. M., Simpson, L. J. and Tarleton, R. L.**, Insufficient TLR activation contributes to the slow development of CD8+ T cell responses in *Trypanosoma cruzi* infection. *J. Immunol.* 2009. **183**: 1245–1252.

2 **Barrias, E. S., Reignault, L. C., De Souza, W. and Carvalho, T. M.**, Dynasore, a dynamin inhibitor, inhibits *Trypanosoma cruzi* entry into peritoneal macrophages. *PLoS One*. 2010. **5**: e7764.

3 **Pena, D. A., Eger, I., Nogueira, L., Heck, N., Menin, Á., Báfica, A. and Steindel, M.**, Selection of TcII *Trypanosoma cruzi* population following macrophage infection. *J. Infect. Dis.* 2011. **204**: 478–486.

4 **Silva, J. S., Morrissey, P. J., Grabstein, K. H., Mohler, K. M., Anderson, D. and Reed, S. G.**, Interleukin 10 and interferon gamma regulation of experimental *Trypanosoma cruzi* infection. *J. Exp. Med.* 1992. **175**: 169–174.

5 **Aliberti, J. C., Machado, F. S., Souto, J. T., Campanelli, A. P., Teixeira, M. M., Gazzinelli, R. T. and Silva, J. S.**, beta-Chemokines enhance parasite uptake and promote nitric oxide-dependent microbiostatic activity in murine inflammatory macrophages infected with *Trypanosoma cruzi*. *Infect. Immun.* 1999. **67**: 4819–4826.

6 **Muñoz-Fernández, M. A., Fernández, M. A. and Fresno, M.**, Synergism between tumor necrosis factor-alpha and interferon-gamma on macrophage activation for the killing of intracellular *Trypanosoma cruzi* through a nitric oxide-dependent mechanism. *Eur. J. Immunol.* 1992. **22**: 301–307.

7 **Hölscher, C., Köhler, G., Müller, U., Mossmann, H., Schaub, G. A. and Brombacher, F.**, Defective nitric oxide effector functions lead to extreme susceptibility of *Trypanosoma cruzi*-infected mice deficient in gamma interferon receptor or inducible nitric oxide synthase. *Infect. Immun.* 1998. **66**: 1208–1215.

8 **Goñi, O., Alcaide, P. and Fresno, M.**, Immunosuppression during acute *Trypanosoma cruzi* infection: involvement of Ly6G (Gr1(+))CD11b(+) immature myeloid suppressor cells. *Int. Immunol.* 2002. **14**: 1125–1134.

9 **Gabrilovich, D. I., Ostrand-Rosenberg, S. and Bronte, V.**, Coordinated regulation of myeloid cells by tumours. *Nat. Rev. Immunol.* 2012. **12**: 253–268.

10 **Voisin, M. B., Buzoni-Gatel, D., Bout, D. and Velge-Roussel, F.**, Both expansion of regulatory GR1+ CD11b+ myeloid cells and anergy of T lymphocytes participate in hyporesponsiveness of the lung-associated immune system during acute toxoplasmosis. *Infect. Immun.* 2004. **72**: 5487–5492.

11 **Arocena, A. R., Onofrio, L. I., Pellegrini, A. V., Carrera Silva, A. E., Paroli, A., Cano, R. C., Aoki, M. P. et al.**, Myeloid-derived suppressor cells are key players in the resolution of inflammation during a model of acute infection. *Eur. J. Immunol.* 2014. **44**: 184–194.

12 **Geissmann, F., Gordon, S., Hume, D. A., Mowat, A. M. and Randolph, G. J.**, Unravelling mononuclear phagocyte heterogeneity. *Nat. Rev. Immunol.* 2010; **10**: 453–460.

13 **Youn, J. I., Kumar, V., Collazo, M., Nefedova, Y., Condamine, T., Cheng, P., Villagra, A. et al.**, Epigenetic silencing of retinoblastoma gene regulates pathologic differentiation of myeloid cells in cancer. *Nat. Immunol.* 2013; **14**: 211–220.

14 **Gonzalez-Juarrero, M., Shim, T. S., Kipnis, A., Junqueira-Kipnis, A. P. and Orme, I. M.**, Dynamics of macrophage cell populations during murine pulmonary tuberculosis. *J. Immunol.* 2003. **171**: 3128–3135.

15 **Idoyaga, J., Suda, N., Suda, K., Park, C. G. and Steinman, R. M.**, Antibody to Langerin/CD207 localizes large numbers of CD8alpha+ dendritic cells to the marginal zone of mouse spleen. *Proc. Natl. Acad. Sci. USA* 2009. **106**: 1524–1529.

16 **Merad, M., Sathe, P., Helft, J., Miller, J. and Mortha, A.**, The dendritic cell lineage: ontogeny and function of dendritic cells and their subsets in the steady state and the inflamed setting. *Annu. Rev. Immunol.* 2013. **31**: 563–604.

17 **Serbina, N. V. and Pamer, E. G.**, Monocyte emigration from bone marrow during bacterial infection requires signals mediated by chemokine receptor CCR2. *Nat. Immunol.* 2006. **7**: 311–317.

18 **Dunay, I. R., Damatta, R. A, Fux, B., Presti, R., Greco, S., Colonna, M. and Sibley, L. D.**, Gr1(+) inflammatory monocytes are required for mucosal resistance to the pathogen *Toxoplasma gondii*. *Immunity*. 2008. **29**: 306–317.

19 **Hohl, T. M., Rivera, A., Lipuma, L., Gallegos, A., Shi, C., Mack, M. and Pamer, E. G.**, Inflammatory monocytes facilitate adaptive CD4 T cell responses during respiratory fungal infection. *Cell Host Microbe*. 2009. **6**: 470–481.

20 **Guilliams, M., Ginhoux, F., Jakubzick, C., Naik, S. H., Onai, N., Schraml, B. U., Segura, E. et al.**, Dendritic cells, monocytes and macrophages: a unified nomenclature based on ontogeny. *Nat. Rev. Immunol.* 2014. **14**: 571–578.

21 **León, B., López-Bravo, M. and Ardavín, C.**, Monocyte-derived dendritic cells formed at the infection site control the induction of protective T helper 1 responses against *Leishmania*. *Immunity*. 2007. **26**: 519–531.

22 **Domínguez, P. M. and Ardavín, C.**, Differentiation and function of mouse monocyte-derived dendritic cells in steady state and inflammation. *Immunol. Rev.* 2010. **234**: 90–104.

23 **Van Overtvelt, L., Vanderheyde, N., Verhasselt, V., Ismaili, J., De Vos, L., Goldman, M., Willems, F. et al.**, *Trypanosoma cruzi* infects human dendritic cells and prevents their maturation: inhibition of cytokines, HLA-DR, and costimulatory molecules. *Infect. Immun.* 1999. **67**: 4033–4040.

24 **Poncini, C. V., Alba Soto, C. D., Batalla, E., Solana, M. E. and González Cappa, S. M.**, *Trypanosoma cruzi* induces regulatory dendritic cells in vitro. *Infect. Immun.* 2008. **76**: 2633–2641.

25 **Poncini, C. V., Ilarregui, J. M., Batalla, E. I., Engels, S., Cerliani, J. P., Cucher, M. A., van Kooyk, Y. et al.**, *Trypanosoma cruzi* Infection Imparts a Regulatory Program in Dendritic Cells and T Cells via Galectin-1-Dependent Mechanisms. *J. Immunol.* 2015. **195**: 3311–3124.

26 **Tamoutounour, S., Guilliams, M., Montanana-Sanchis, F., Liu, H., Terhorst, D., Malosse, C., Pollet, E. et al.**, Origins and functional specialization of macrophages and of conventional and monocyte-derived dendritic cells in mouse skin. *Immunity* 2013. **39**: 925–938.

27 **Seré, K., Baek, J. H., Ober-Blöbaum, J., Müller-Newen, G., Tacke, F., Yokota, Y., Zenke, M. et al.**, Two distinct types of Langerhans cells populate the skin during steady state and inflammation. *Immunity* 2012. **37**: 905–916.

28 **Guilliams, M., Movahedi, K., Bosschaerts, T., VandenDriessche, T., Chuah, M. K., Hérin, M., Acosta-Sanchez, A. et al.**, IL-10 dampens TNF/inducible nitric oxide synthase-producing dendritic cell-mediated pathogenicity during parasitic infection. *J. Immunol.* 2009. **182**: 1107–1118.

29 **Segura, E. and Amigorena, S.**, Inflammatory dendritic cells in mice and humans. *Trends Immunol.* 2013. **34**: 440–445.

30 **Shi, C. and Pamer, E. G.**, Monocyte recruitment during infection and inflammation. *Nat. Rev. Immunol.* 2011. **11**: 762–774.

31 **Morias, Y., Abels, C., Laoui, D., Van Overmeire, E., Guilliams, M., Schouppe, E., Tack, F. et al.**, Ly6C- Monocytes Regulate Parasite-Induced Liver Inflammation by Inducing the Differentiation of Pathogenic Ly6C+ Monocytes into Macrophages. *PLoS Pathog* 2015. **11**: e1004873.

32 **Batalla, E. I., Pino Martínez, A. M., Poncini, C. V., Duffy, T., Schijman, A. G., González Cappa, S. M. and Alba Soto, C. D.**, Impairment in natural killer cells editing of immature dendritic cells by infection with a virulent *Trypanosoma cruzi* population. *J. Innate. Immun.* 2013. **5**: 494–504.

33 **León, B. and Ardavín, C.**, Monocyte migration to inflamed skin and lymph nodes is differentially controlled by L-selectin and PSGL-1. *Blood* 2008. **111**: 3126–3130.

34 **Jakubzick, C., Gautier, E. L., Gibbings, S. L., Sojka, D. K., Schlitzer, A., Johnson, T. E., Ivanov, S. et al.**, Minimal differentiation of classical monocytes as they survey steady-state tissues and transport antigen to lymph nodes. *Immunity* 2013. **39**: 599–610.

35 **Geissmann, F., Jung, S. and Littman, D. R.**, Blood monocytes consist of two principal subsets with distinct migratory properties. *Immunity* 2003. **19**: 71–82.

36 **Menezes, S., Melandri, D., Anselmi, G., Perchet, T., Loschko, J., Dubrot, J., Patel, R. et al.**, The Heterogeneity of Ly6Chi Monocytes Controls Their Differentiation into iNOS+ Macrophages or Monocyte-Derived Dendritic Cells. *Immunity* 2016. **45**: 1205–1218.

37 **Briseño, C. G., Haldar, M., Kretzer, N. M., Wu, X., Theisen, D. J., Kc, W., Durai, V. et al.**, Distinct Transcriptional Programs Control Cross-Priming in Classical and Monocyte-Derived Dendritic Cells. *Cell Rep.* 2016. **15**: 2462–2474.

38 **Bosschaerts, T., Guilliams, M., Stijlemans, B., Morias, Y., Engel, D., Tacke, F., Hérin, M. et al.**, Tip-DC development during parasitic infection is regulated by IL-10 and requires CCL2/CCR2, IFN-gamma and MyD88 signaling. *PLoS Pathog* 2010. **6**: e1001045.

39 **Sponaas, A. M., Freitas do Rosario, A. P., Voisine, C., Mastelic, B., Thompson, J., Koernig, S., Jarra, W. et al.**, Migrating monocytes recruited to the spleen play an important role in control of blood stage malaria. *Blood* 2009. **114**: 5522–5531.

40 **Zigmond, E., Varol, C., Farache, J., Elmaliah, E., Satpathy, A. T., Friedlander, G., Mack, M. et al.**, Ly6C hi monocytes in the inflamed colon give rise to proinflammatory effector cells and migratory antigen-presenting cells. *Immunity* 2012. **37**: 1076–1090.

41 **Meredith, M. M., Liu, K., Kamphorst, A. O., Idoyaga, J., Yamane, A., Guermonprez, P., Rihn, S. et al.**, Zinc finger transcription factor zDC is a negative regulator required to prevent activation of classical dendritic cells in the steady state. *J Exp Med.* 2012. **209**: 1583–1593.

42 **Greter, M., Helft, J., Chow, A., Hashimoto, D., Mortha, A., Agudo-Cantero, J., Bogunovic, M. et al.**, GM-CSF controls nonlymphoid tissue dendritic cell homeostasis but is dispensable for the differentiation of inflammatory dendritic cells. *Immunity* 2012. **36**: 1031–1046.

43 **Cuervo, H., Guerrero, N. A., Carbajosa, S., Beschin, A., De Baetselier, P., Gironès, N. and Fresno, M.**, Myeloid-derived suppressor cells infiltrate the heart in acute *Trypanosoma cruzi* infection. *J. Immunol.* 2011. **187**: 2656–2665.

44 **Heil, M., Ziegelhoeffer, T., Pipp, F., Kostin, S., Martin, S., Clauss, M. and Schaper, W.**, Blood monocyte concentration is critical for enhancement of collateral artery growth. *Am. J. Physiol. Heart Circ. Physiol.* 2002. **283**: H2411-2419.

45 **Vincent, J., Mignot, G., Chalmin, F., Ladoire, S., Bruchard, M., Chevriaux, A., Martin, F. et al.**, 5-Fluorouracil selectively kills tumor-associated myeloid-derived suppressor cells resulting in enhanced T cell-dependent antitumor immunity. *Cancer Res.* 2010. **70**: 3052–3061.

46 **Geissmann, F., Manz, M. G., Jung, S., Sieweke, M. H., Merad, M. and Ley, K.**, Development of monocytes, macrophages, and dendritic cells. *Science* 2010. **327**: 656–661.

47 **Brudecki, L., Ferguson, D. A., McCall, C. E. and El Gazzar, M.**, Myeloid-derived suppressor cells evolve during sepsis and can enhance or attenuate the systemic inflammatory response. *Infect. Immun.* 2012. **80**: 2026–2034.

48 **De Trez, C., Magez, S., Akira, S., Ryffel, B., Carlier, Y. and Muraille, E.**, iNOS-producing inflammatory dendritic cells constitute the major infected cell type during the chronic *Leishmania major* infection phase of C57BL/6 resistant mice. *PLoS Pathog.* 2009. **5**: e1000494.

49 **Schuler, G. and Steinman, R. M.**, Murine epidermal Langerhans cells mature into potent immunostimulatory dendritic cells in vitro. *J. Exp. Med.* 1985. **161**: 526–546.

Abbreviations: **DCs**: Dendritic cells · **iDC-like**: inflammatory-like DCs · **LCs**: Langerhans cells · **Mo-DCs**: Mo-derived DCs · **Mo**: monocytes · **MDSCs**: myeloid–derived suppressor cells · **Tp**: trypomastigotes · **iNOS**: inducible nitric oxide synthase · **NO**: nitric oxide · **BM**: bone marrow · **dLNs**: draining lymph nodes · **dpi**: days post-infection · **hpi**: hours post-infection · **id**: intradermic · **5-FU**: 5-fluorouracil · **NI**: not-infected · **IFN-γ**: interferon gamma · **TNF-α**: tumor necrosis factor-alpha

Full correspondence: Dr. Carolina Verónica Poncini. Paraguay 2155, Piso 13, Facultad de Medicina, Universidad de Buenos Aires. CP 1121, Ciudad Autónoma de Buenos Aires. Argentina
e-mail: cvponcini@gmail.com

Received: 23/11/2016
Revised: 22/5/2017
Accepted: 5/7/2017
Accepted article online: 27/7/2017

